

### Journal of Biomolecular Structure and Dynamics



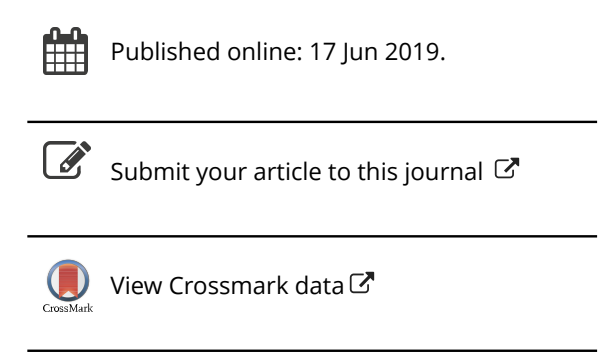
ISSN: 0739-1102 (Print) 1538-0254 (Online) Journal homepage: https://www.tandfonline.com/loi/tbsd20

# S100A4: a novel partner for heat shock protein 47 in antler stem cells and insight into the calcium ion-induced conformational changes

Yudong Shang, Zhengyao Zhang, Hengxing Ba, Datao Wang, Xiaoyan Qi & Chunyi Li

**To cite this article:** Yudong Shang, Zhengyao Zhang, Hengxing Ba, Datao Wang, Xiaoyan Qi & Chunyi Li (2019): S100A4: a novel partner for heat shock protein 47 in antler stem cells and insight into the calcium ion-induced conformational changes, Journal of Biomolecular Structure and Dynamics, DOI: 10.1080/07391102.2019.1630002

To link to this article: <a href="https://doi.org/10.1080/07391102.2019.1630002">https://doi.org/10.1080/07391102.2019.1630002</a>







# S100A4: a novel partner for heat shock protein 47 in antler stem cells and insight into the calcium ion-induced conformational changes

Yudong Shang<sup>a</sup>, Zhengyao Zhang<sup>b</sup>, Hengxing Ba<sup>a</sup>, Datao Wang<sup>a</sup>, Xiaoyan Qi<sup>a</sup> and Chunyi Li<sup>a</sup>

<sup>a</sup>Institute of Special Wild Economic Animals and Plants, Chinese Academy of Agricultural Sciences, and State Key Laboratory for Molecular Biology of Special Economic Animals, Changchun, People's Republic of China; <sup>b</sup>School of Life Science and Medicine, Dalian University of Technology, Panjin, People's Republic of China

Communicated by Ramaswamy H. Sarma

#### **ABSTRACT**

S100A4 is a multiple-function protein highly expressed in tumor or stem cells. We found S100A4 was a novel protein partner for heat shock protein 47 (HSP47) in deer antlerogenic periosteum cells (AP cells), indicating that \$100A4 could bind with HSP47. \$100A4 had both calcium-dependent and calcium-independent patterns (labeled as SCd and SCi, respectively) to execute different biological activities. Homology models of HSP47, SCd and SCi were constructed. HSP47:collagen model, HSP47:collagen I-V, HSP47:SCd and HSP47:SCi complexes were built using ZDOCK software. Together with free SCd and SCi, 200 ns molecular dynamic (MD) simulations were performed to analyze binding free energies and SCi/SCd conformational changes. The energetic results showed that SCi had the strongest affinity to HSP47, and followed by collagens. SCd had little interaction with HSP47. Decomposition energy results showed that collagen model interacted with HSP47 mainly though neutral amino acids. When SCi bound with HSP47, the majority of mediated amino acids were charged. These results indicated that SCi could compete with collagen on the binding site of HSP47. Root mean square fluctuation (RMSF) values and cross-correlation matrices of principal component analysis (PCA) were calculated to evaluate the SCi/SCd structural variation during MD simulation. Both HSP47 and Ca<sup>2+</sup> could stabilize the conformation of SCi/SCd. The loops interacting with Ca<sup>2+</sup>s and linking the two EF-hand motifs were impacted particularly. The relative moving directions of α-helices in EFhands were distinct by the binding effect of HSP47 and Ca<sup>2+</sup>. We found that SCi may regulate the differentiation of AP cells by disturbing the interaction between HSP47 and collagen.

**Abbreviations:** aECO: Antler endochondral ossification; AP: Antlerogenic periosteum;  $\Delta G_{\rm bind}$ : Binding free energies; BM: Basement membrane; CG: Conjugate gradient; DMEM: Dulbecco's Modified Eagle's Medium; GGB: Electrostatic solvation free energy; ESC: Embryonic stem cell; ER: Endoplasmic reticulum; EMT: Epithelial-to-mesenchymal transition; EEF1A1: Eukaryotic translation elongation factor  $1-\alpha1$ ; ECM: Extracellular matrix; FBS: Fetal bovine serum; GB: Generalized Born; HSP47: Heat shock protein 47; IMO: Intramembranous ossification; LJ: Lennard-Jones; LC-MS/MS: Liquid chromatography-tandem mass spectrometry; MALDI-IMS: Matrix-assisted laser desorption/ionization imaging mass spectrometry; MMP: Matrix metalloproteinase; MD: Molecular dynamic; MM-GB/SA: Molecular Mechanics with a generalized Born/Surface Area solvent; GSA: Nonpolar solvation free energy; OPC: Ossification pattern change; PME: Particle Mesh Ewald; pECO: Pedicle endochondral ossification; PP: Pedicle periosteum; PMF: Peptide mass fingerprinting; PCA: Principal component analysis; RLP4: Ribosomal protein L4; RM: Reserve mesenchyme; RMSF: Root mean square fluctuation; RMSD: Root-mean-square deviation; SCd: S100A4 of calcium-dependent; SMC: Secondary mesenchyme cell; Gsol: Solvation energy; SASA: Solvent accessible surface area; SD: Steepest descent

#### **ARTICLE HISTORY**

Received 31 August 2018 Accepted 20 May 2019

#### **KEYWORDS**

S100A4; HSP47; proteinprotein docking; molecular dynamics; antler stem cell

#### Introduction

S100A4 is an 11.5 kDa sequence-conserved protein, and belongs to the S100 family with the EF-hand Ca<sup>2+</sup>-binding motifs. Like other members of S100 family, S100A4 exists as a dimer to regulate the activities of protein partners, mainly through affecting localization or accessibility of these partners (Helfman, Kim, Lukanidin, & Grigorian, 2005; Kim & Helfman, 2003; Schmidt-Hansen et al 2004; Tarabykina et al., 2007). Calcium-dependent conformational change is

necessary for S100 proteins to interact with their targets and execute biological activities. S100 contains a highly conserved calcium-binding loop on both end of which are followed by an  $\alpha$ -helix, respectively. The helix-loop-helix motif is called EF-hand (Santamaria-Kisiel, Rintala-Dempsey, & Shaw, 2006). S100A4 has been reported capable of both calcium-dependent and calcium-independent patterns (marked as SCd and SCi, respectively), which interact with different target molecules (Santamaria-Kisiel et al., 2006). S100A4

Maelandsmo, 2010).

Gene Serpin H1 encodes heat shock protein 47 (HSP47), which is a 47 kDa protein and belongs to a member of the evolutionarily conserved serpin family, a superfamily of plasma serine protease inhibitors, but lacks the active site essential for the inhibition of proteases (Hirayoshi et al., 1991). This protein is reportedly expressed in response to various types of stress in different pathological and physiological processes (Minowada & Welch, 1995; Widmer et al., 2012). During the maturation of collagens, HSP47 can bind to type I-V pro-collagens as a protein chaperon once the complex co-translocated into the endoplasmic reticulum (ER) and facilitates the assembly/secretion of collagen (Chu et al., 2015; Nagata, 1998). It is reported that HSP47 expressed in antlerogenic periosteum (AP) cells using matrix-assisted laser desorption/ionization imaging mass spectrometry (MALDI-IMS) (Deb-Choudhury et al., 2015). Besides, HSP47 was highly expressed in embryonic stem cell (ESC) and participated in differentiating into the secondary mesenchyme cell (SMC) lineages (Wong et al., 2014). Similar to S100A4, increased HSP47 expression is associated with higher cancer stage and shorter recurrent-free survival (Xu, 2015).

In previous publications (Goss, 1990; Li, Mackintosh, Martin, & Clark, 2007a; Wang, Chu, Sun, Ba, & Li, 2017), we reported that \$100A4 protein is highly expressed in the AP, the pedicle (permanent bony protuberance from which an antler casts and regenerates) periosteum (PP) and reserve mesenchyme (RM) in a growing antler tip. The latter two are the further differentiated progeny of the AP. A combination of tissue deletion and transplantation experiments demonstrated that potential of initial formation of a pedicle and first antler only resides in the AP: deletion of the AP abrogates future pedicle and antler formation; whereas, transplantation of the AP elsewhere on the deer body induces ectopic pedicle and antler growth. It is known that the PP is the exclusive tissue type responsible for annual antler regeneration (Li, Yang, & Suttie, 2011; Li, Zhao, Liu, & Mcmahon, 2014; Li et al., 2007b). Further research finds that both the AP cells and the PP cells express some key embryonic stem cell markers, such as Oct4, Nanog and Sox2; and can be induced to differentiate into multiple somatic cell types, such as chondrocytes, osteoblasts, myocytes and adipocytes (Li, Yang, & Sheppard, 2009). Therefore, the AP cells are termed stem cells for antler generation, and the PP cells stem cells for antler regeneration.

Because expression level of S100A4 is maintained at the same level throughout the differentiation ontogeny from the AP cells to the PP cells (Li et al., 2009), our findings are different from those discoveries in the cancer cell research, in

which increasing expression of \$100A4 would promote cancer cell invasion and metastasis. Hence, revealing the mechanism underlying the change in expression level of \$100A4 during transition from the AP cells to the PP cells may help to decipher the role played by \$100A4 in cancer progression.

The aim of the present study was to use the techniques of co-immunoprecipitation to firstly identify the partner proteins for \$100A4, and then to carry out the molecular dynamics simulations to investigate the interactions between these partner proteins and resulted conformational changes. In so doing to explore the molecular mechanism of antler development.

#### **Materials and methods**

## AP cells collection, culture, and co-immunoprecipitation assay

The AP prior to the initiation of pedicle formation was obtained from the slaughtered male sika deer under 56 kg (Li, Clark, Lord, Stanton, & Suttie, 2002). The deer tissue wasfor isolating cells and for primary cell culturing. The AP tissue collection from sika deer was approved by CAAS animal ethics committee (CAAS201523). All of the cell types were cultured in Dulbecco's Modified Eagle's Medium (DMEM) (Gibco; Grand Island), and supplemented with 10% fetal bovine serum (FBS),  $100 \, \text{mg} \cdot \text{mL}^{-1}$  of streptomycin, and  $100 \, \mu \cdot \text{mL}^{-1}$  of penicillin, and grown in a humidified atmosphere with 5% CO<sub>2</sub> at 37 °C.

Cells were seeded at the density of  $1 \times 10^6$  in a 60 mm culture dish and cultured under hypoxic conditions (1%  $O_2$ , 94%  $N_2$ , and 5%  $CO_2$ ), then, lysed in RIPA buffer. The proteins were collected. Thirty micrograms of the protein samples were incubated for 12 h with  $10\,\mu\text{L}$  pre-incubated anti-S100A4 (10 kD, 1:1000, Santa Cruz) magnetic beads according to the manufacturer's protocol. The complexes were washed for five times to elute non-specific and non-cross-linked antibodies. The precipitated proteins were resuspended in  $30\,\mu\text{L}$  SDS sample buffer and boiled at 95 °C for  $10\,\text{min}$ . The immune complexes were precipitated, separated and identified on a one-dimensional SDS PAGE gel.

#### **Mass spectrometry**

To identify the binding protein of S100A4, liquid chromatography-tandem mass spectrometry (LC-MS/MS) was used. The injection volume of lysed product was 6  $\mu$ L. Liquid phase A was 0.1% formic acid dissolved in 2% methyl myanide aqueous solution. Liquid phase B was 0.1% formic acid dissolved in 84% methyl myanide aqueous solution. The EASY column SC200 150  $\mu$ m  $\times$  100 mm (RP-C<sub>18</sub>) was then equilibrated with 100% A (Thermo). The chromatographic separation was performed on the C<sub>18</sub> column using autosampler (EASY-nLC1000). The column temperature was kept at 20 °C, and the autosampler was maintained at 4 °C. The flow was 400 nL·min<sup>-1</sup>. The related elution gradient was below: 0–100 min, the linear gradient of B was raised from 0% to 45%; 100–108 min, the linear gradient of B was raised from 45% to

100%; 108-120 min, the concentration of B maintained 100%. The separated products were analyzed using Q-Exactive MS (Thermo Finnigan). Analyzing time: 120 min; monitoring mode: positive ion; scanning range of parent ion: 300–1800 m/z. Twenty fragmentation patterns were collected after every full scanning (MS<sup>2</sup> scan, HCD). The resolution of  $MS^1$  on m/z 200 was 70,000. The resolution of  $MS^2$  on m/z200 was 17,500. Maxquant 1.3.0.5 and Perseus 1.3.0.4 softwares were used to perform the non-scalar quantity analysis, statistics and bioinformatics analysis, respectively.

#### Homology modeling and docking study

We searched HSP47 and S100A4 sequences belonging to Cervidae from NCBI database (http://www.ncbi.nlm.nih.gov, protein ID: XP 020769256.1, XP 020746513.1, respectively) to build homology model. Besides, we also selected collagen I-V sequences in NCBI (protein ID: NP 000079.2, NP 001835.3, NP\_000081.1, NP\_001836.3, and NP\_001265003.1 respectively) to perform homology modeling. Sequence alignment and homology modeling was carried out on Swiss-Model (Biasini et al., 2014) website (https://www.swissmodel.expasy. org/). The three-dimensional structures of HSP47 and S100A4 were then constructed based on the crystal structure of collagen-specific chaperone HSP47 SERPINH1, chain A (PDB code: 3ZHA) and TFP-Ca<sup>2+</sup>-bound activated form of the S100A4, chain A (PDB code: 3KO0), respectively. The collagen I-V structures were constructed based on the crystal structure of an abc collagen heterotrimer (PDB code: 2KLW). After modeling, the structures were checked by QMEAN Score and QMEANDisCo score (Benkert, Biasini, & Schwede, 2011). The QMEAN Score provides an estimate of the 'degree of nativeness' of the structural features observed in the model on a global scale. QMEANDisCo score assesses the consistency of observed interatomic distances in each residue of the model with ensemble information extracted from experimentally determined protein structures that are homologues to the target sequence. The collagen model was from the crystal structure (PDB code: 3ZHA), which is a homotrimeric synthetic model. An important residue arginine within the Xaa-Arg-Gly triplet sequence is recognized by a conserved aspartic acid of HSP47 (Widmer et al., 2012). We further utilized the AMBER14 software package (Case, Berryman, & Betz, 2015) to execute a minimization of 400-step steepest descent (SD) and 600-step conjugate gradient (CG) to relax the homology modeling structures and collagens. 12-6 Lennard-Jones (LJ) nonbonded method (Li, Roberts, Chakravorty, & Merz, 2013) was used for the models containing Ca<sup>2+</sup>s, and the ff99sb force field (Hornak et al., 2006) was applied for energy minimization. After minimization, Ramachandran plot analysis (Laskowski, Macarthur, Moss, & Thornton, 1993) examined the reliability of the backbone torsion angles  $(\Phi - \Psi)$  of the refined proteins.

ZDOCK software 3.0.2 (Pierce, Hourai, & Weng, 2011) was used to perform the docking simulation of collagens, and S100A4 with HSP47. Ten top docking poses were generated. The cutoff value of root-mean-square deviation (RMSD) was 1.0 Å, and interface cutoff value was 2.0 Å. Zrank scoring algorithm was then tested on ZDOCK benchmark dataset version 4.0 (Hwang, Vreven, Janin, & Weng, 2010). The binding residues interacting with collagens were predefined according to the crystal structure of 3ZHA. The binding site of S100A4 and HSP47 was not defined.

#### Molecular dynamics (MD) simulation

All the MD simulations were performed on HP DL980 server using the AMBER14. 12-6 LJ nonbonded model was established for the structures with Ca2+s. The ff99sb force field was used for energy minimization and MD simulations. The charges of the structures above were neutralized using tleap module of AMBER14. An explicit solvent model TIP3P water box (Jorgensen, Chandrasekhar, Madura, Impey, & Klein, 1983) was used with distance of 12.0 Å between protein surface and water box boundary. A minimization of 1000-step SD and 1000-step CG was carried out. The constraint force constant on proteins was 500 kcal·mol<sup>-1</sup>·Å<sup>-2</sup>. After that, without any restraint on the whole system, a minimization of 3000-step SD and 4000-step CG was used. Then, a heating simulation was performed from 0 to 300 K in 500 ps with a weak constraint force constant value of  $10.0 \text{ kcal·mol}^{-1} \cdot \mathring{A}^{-2}$ . After heating, a NPT ensemble of 1 atm and 300 K was applied for 200 ns equilibrium simulation without any constraint. Periodic boundary condition was used to the system to obtain consistent behavior. The cutoff value of nonbonded interaction was 12.0 Å. The particle mesh ewald (PME) method (Essmann et al., 1995) was employed for the computation of long-range electrostatic forces. The bond lengths of hydrogen-heavy atoms were constrained using the SHAKE algorithm (Coleman, Mesick, & Darby, 1977). The time step was 2.0 fs. A simple Leapfrog integrator was used to propagate the dynamics, with the collision frequency of 1.0 ps<sup>-1</sup>. A Langevin thermostat was adopted. The relaxation time for barostat bath was 2.0 ps. VMD (Humphrey, Dalke, & Schulten, 1996) software was used to visualize the trajectories and to depict structural representations.

#### The calculations of binding free energy

Molecular Mechanics with a Generalized Born/Surface Area solvent (MM-GB/SA) (Miller et al., 2012) method implemented in AMBER14 was applied to calculate the binding free energy between the ligand and the receptor (Swanson, Henchman, & Mccammon, 2004). The binding free energies ( $\Delta G_{\text{bind}}$ ) in MM-GB/SA between a ligand (collagen/S100A4) and a receptor (HSP47) were calculated as:

$$\Delta G_{\text{bind}} = G_{\text{complex}} - G_{\text{receptor}} - G_{\text{ligand}} \tag{1}$$

$$G = E_{MM} + G_{sol} - TS \tag{2}$$

$$E_{\rm MM} = E_{\rm int} + E_{\rm ele} + E_{\rm vdw} \tag{3}$$

$$G_{\rm sol} = G_{\rm GB} + G_{\rm SA} \tag{4}$$

In Equation (2), the  $E_{\rm MM}$ ,  $G_{\rm sol}$ , and TS represented molecular mechanics component in gas phase, the stabilization energy due to solvation, and a vibrational entropy term,

respectively.  $E_{\rm MM}$  was given as a sum of  $E_{\rm int}$ ,  $E_{\rm ele}$ , and  $E_{\rm vdw}$  which were internal, coulomb and van der Waals interaction terms, respectively. Solvation energy  $(G_{\rm sol})$  was separated into an electrostatic solvation free energy  $(G_{\rm SA})$  and a nonpolar solvation free energy  $(G_{\rm SA})$ . The former could be obtained from the Generalized Born (GB) method. The latter was considered to be proportional to the molecular solvent accessible surface area (SASA) (Hou, Zhang, Case, & Wang, 2008). The binding free energies were obtained by averaging over the values calculated for 2000 snapshots from the last 20 ns of the trajectories at 5 ps intervals for the complex structures.

#### Principal component analysis (PCA)

The MD trajectories in this work were further investigated using PCA method (Duan, Feng, & Zhang, 2016) to probe conformational changes of S100A4 molecules in the MD trajectories. PCA analysis was carried out using the CPPTRAJ module (Roe & Cheatham, 2013) implemented in AMBER14. PCA allowed identification of essential degrees of freedom in the motions of proteins. This method involved the construction of the covariance matrix of atomic coordinates from MD trajectories. The eigenvectors and eigenvalues, representing concerted motions of proteins, could be obtained by diagonalising the covariance matrix. The eigenvectors described the directions of motions, while the corresponding eigenvalues indicated amplitudes of motions along these eigenvectors. The first few principal components were generally considered as the ones representing functionally significant motions of proteins. In addition, the cross-correlation map (Chen, Wang, Zhu, Zhang, & Zhang, 2015; Ichiye, & Karplus, 1991) was also computed using MD trajectories to explore internal dynamics of S100A4. The cross-correlation coefficient  $C_{ii}$  of each pair of  $C_{\alpha}$  atoms i and j was determined using the following equation:

$$C_{ij} = \frac{\langle \Delta r_i \cdot \Delta r_j \rangle}{\left(\langle \Delta r_i^2 \rangle \langle \Delta r_j^2 \rangle\right)^{1/2}}$$
 (5)

where  $\Delta r_i$  indicated that the displacement from the average position of the ith atom. The values of matrix elements  $C_{ij}$  changed between -1 and 1. The positive  $C_{ij}$  depicted correlated motions of residue i relative to j, while the negative  $C_{ij}$  represented anticorrelated motions between residues i and j.

#### Results

#### HSP47 is one of the binding partner of S100A4

A co-immunoprecipitation experiment utilized native protein from the AP cells was carried out. There were no antibodies added in the control (No Ab-column). The AP cells-column showed that S100A4 was co-precipitated with  $\alpha$  and  $\beta$ -tubulin, Serpin H1 (HSP47), eukaryotic translation elongation factor 1- $\alpha$ 1 (EEF1A1) and ribosomal protein L4 (RPL4) (Figure 1). Among these complexes, the band of HSP47:S100A4:anti-S100A4 complex was highlighted ( $\sim$ 70 kD). In contrast, other protein

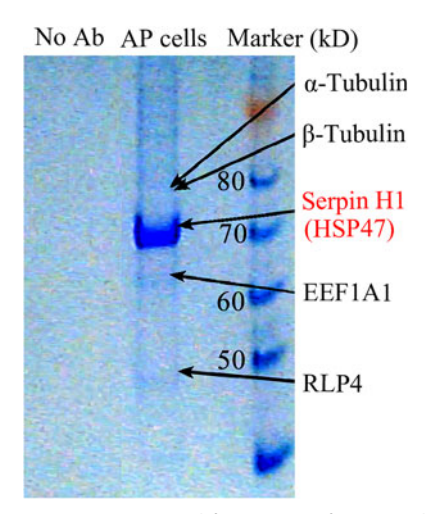


Figure 1. Co-immunoprecipitation gel for partners of S100A4. The APCs equals AP cells.

candidates did not show specific affinity towards S100A4. We further performed LC-MS/MS to qualify HSP47 binding with S100A4. Twelve primitive files were imported in Maxquant software. The database was P17031\_420\_20170214\_modified.fasta, including 420 sequences. The peptide mass fingerprinting (PMF) maps of the protein spots were obtained (Figure 2). The sequence fragments were coincidental with the amino acid alignments of HSP47 and S100A4 (Supporting Information Figure S1A, C).

## Homology modeling and docking study of HSP47 and S100A4

Swiss-Model was applied to perform HSP47 and S100A4 homology modeling. The results showed that the sequences of HSP47 and S100A4 shared high homology with the tem-(98.2% and 96.0%, respectively) (Supporting plates Information Figure S1A, C). There were 99.2% and 96.8% QMEANDisCo scores higher than 0.6 (Supporting Information Figure S1B, D) in HSP47 and S100A4 models, respectively. After minimization, the Ramachandran plots showed that 99.2% and 99.4% of the  $\theta\text{-}\phi$  angles in the refined HSP47 and \$100A4 models lay in the allowed region (Supporting Information Figure S2). The sequence alignment of collagen I-V had 55.17%, 55.68%, 56.04%, 61.54%, and 60.47% identities with the template. The QMEAN scores were -0.98 for HSP47 and -1.18 for S100A4, 2.39, 2.78, 3.16, 3.16, and 3.29 for collagen I–V, respectively (Supporting Information Figure S3). The QMEANDisCo scores were 97.8%, 96.7%, 95.8%, 97.0%, and 97.8% higher than 0.6 in collagen I-V models (Supporting Information Figure S3). All the Ramachandran plots of collagen I-V were in the acceptable region (Supporting Information Figure S3). These results mean that the homology models were reliable. The small molecules in HSP47 and S100A4 were deleted. We obtained HSP47, S100A4 with four Ca<sup>2+</sup> ions (SCd) and S100A4 without any Ca<sup>2+</sup> ion (SCi) molecules.

After homology modeling and structural refinement, we docked collagens, SCi and SCd on HSP47, respectively (Figure 3, Supporting Information Figure S4). Subsequently,

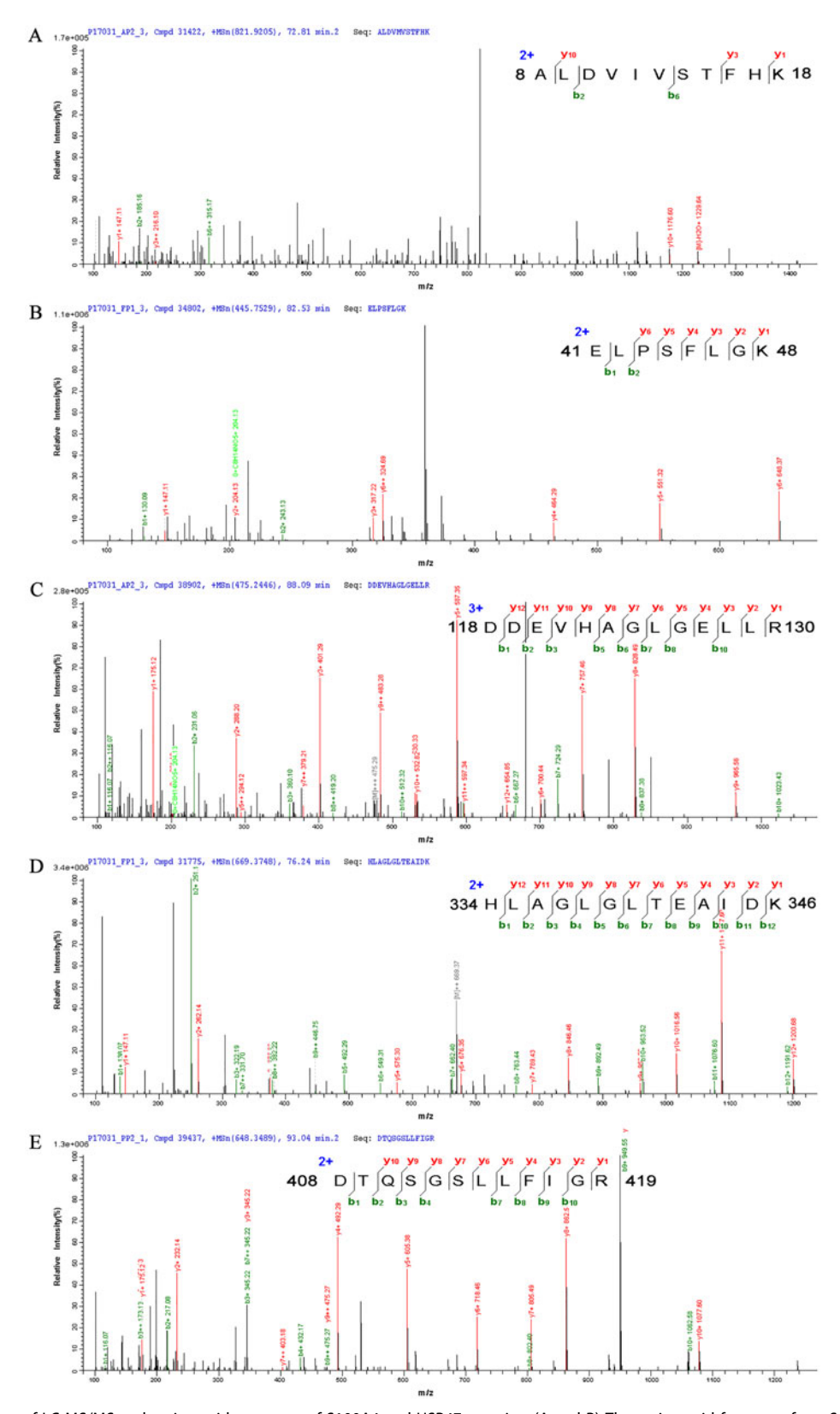


Figure 2. The m/z values of LC-MS/MS and amino acid sequence of S100A4 and HSP47 proteins. (A and B) The amino acid fragment from S100A4. (C-E) The amino acid fragment from HSP47.

HSP47:collagen model complex was superimposed with the crystal structure (PDB code: 3ZHA, Figure 3(A)), the RMSD value was 0.322 Å, indicating the docking method was receivable. Docking results (Figure 3(C,E)) showed that the respective docked SCi and SCd occupied the same binding site of HSP47, which interacted with collagens. The zrank scores were -102.61 for HSP47:collagen model, -98.85 for HSP47:SCi, -98.05 for HSP47:SCd, -105.86, -101.47, -103.76, -103.68, and -101.24 for HSP47:collagen I-V complexes, respectively. The eight complexes were constructed.

#### Analysis of MD trajectories and binding free energy

After 200 ns MD simulation, the average RMSD values of HSP47:collagen model, HSP47:SCi, HSP47:SCd, HSP47:collagen I-V complexes were 2.30 Å, 3.56 Å, 3.48 Å (Figure 4(A)), 1.69 Å, 1.79 Å, 1.62 Å, 1.67 Å, and 1.74 Å (Supporting Information Figure S3), respectively. The values of free SCi, free SCd, SCi, and SCd subunits from the complexes were 3.34 Å, 1.97 Å, 2.98 Å, and 1.86 Å, respectively (Figure 4(B)).

The analysis of binding free energies showed that obvious differences of binding affinity were found among these eight complexes below from strongest to the weakest: HSP47 and SCi  $(-37.87 \text{ kcal} \cdot \text{mol}^{-1})$ , collagen IV  $(-15.21 \text{ kcal} \cdot \text{mol}^{-1})$ , collagen model  $(-12.04 \text{ kcal} \cdot \text{mol}^{-1})$  collagen V  $(-10.65 \text{ kcal} \cdot \text{mol}^{-1})$ , collagen III (-7.58 kcal·mol<sup>-1</sup>), collagen I (-6.56 kcal·mol<sup>-1</sup>), collagen (-0.67 kcal·mol-1), SCd  $(4.39 \text{ kcal·mol}^{-1})$ , respectively (Table 1).

Decomposition energy contributed by each interacting residue was listed for HSP47:collagen model and HSP47:SCi, respectively (Tables 2-3). In the HSP47:collagen model complex, most of the residues were nonpolar prolines, and the

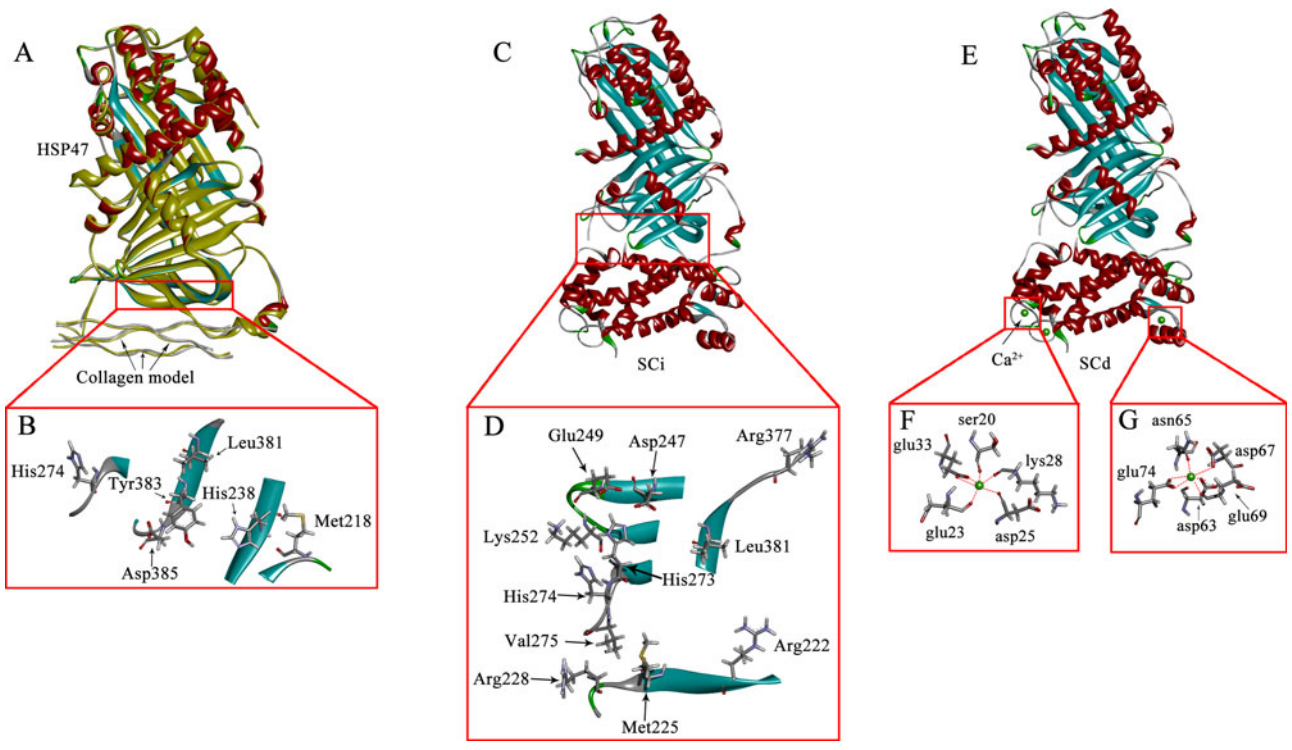


Figure 3. (A) The docking structure of HSP47:collagen complex (color) and the superimpose with the crystal structure (PDB code: 3ZHA, yellow). (B) The key residues of HSP47 interacting with collagen model. (C) The docking structure of HSP47:SCi. (D) The key residues of HSP47 interacting with SCi. (E) The docking structure ture of HSP47:SCd. (F and G) The residues interacting with Ca<sup>2+</sup>.

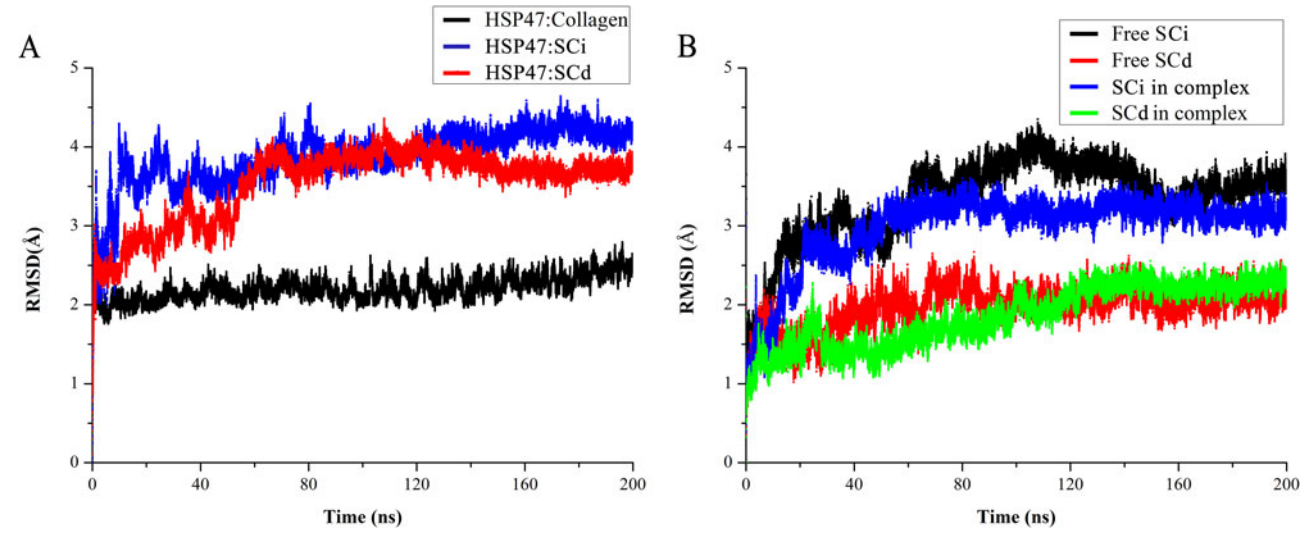


Figure 4. (A) The RMSD plots of HSP47:collagen, HSP47:SCi and HSP47:SCd complexes within 200 ns simulation. (B) The RMSD plots of different SCi/SCd molecules within 200 ns simulation.

Table 1. Binding free energies (kcal·mol<sup>-1</sup>) and its components between HSP47 and collagen/SCi/SCd.

System	$E_{ m vdw}$	$E_{ m ele}$	$\Delta G_{GB}$	$\Delta G_{SASA}$	$\Delta G_{MM-GB/SA}^{a}$	−TΔS	$\Delta G_{tot}{}^{b}$
HSP47:collagen model	-56.98 ± 4.28	-152.63 ± 5.29	201.15 ± 6.94	$-8.63 \pm 0.78$	$-17.09 \pm 0.60$	$5.05 \pm 0.54$	$-12.04 \pm 2.30$
HSP47:SCi	$-70.39 \pm 7.90$	$-816.38 \pm 61.58$	$854.70 \pm 58.99$	$-11.96 \pm 0.96$	$-44.03 \pm 9.13$	$6.16 \pm 1.00$	$-37.87 \pm 3.35$
HSP47:SCd	$-71.21 \pm 8.78$	$-275.39 \pm 49.31$	$356.42 \pm 44.45$	$-10.67 \pm 1.20$	$-0.85 \pm 0.83$	$5.24 \pm 0.58$	$4.39 \pm 1.31$
HSP47:collagen I	$-32.74 \pm 1.18$	$-176.52 \pm 8.06$	$212.26 \pm 9.79$	$-12.51 \pm 1.10$	$-9.51 \pm 1.02$	$2.95 \pm 0.91$	$-6.56 \pm 1.83$
HSP47:collagen II	$-29.62 \pm 0.35$	$-183.50 \pm 6.11$	$210.80 \pm 6.24$	$-10.01 \pm 1.21$	$-12.33 \pm 1.58$	$1.66 \pm 0.14$	$-10.67 \pm 2.42$
HSP47:collagen III	$-31.43 \pm 0.80$	$-189.65 \pm 8.19$	$225.86 \pm 11.56$	$-15.16 \pm 1.44$	$-10.38 \pm 1.31$	$2.80 \pm 0.19$	$-7.58 \pm 1.91$
HSP47:collagen IV	$-45.44 \pm 1.69$	$-166.09 \pm 9.89$	$209.73 \pm 8.73$	$-17.93 \pm 3.05$	$-19.73 \pm 2.68$	$4.52 \pm 0.93$	$-15.21 \pm 2.11$
HSP47:collagen V	$-42.32 \pm 2.44$	-167.11 ± 7.97	$207.67 \pm 7.78$	-16.41 ± 1.91	-18.17 ± 1.72	$7.52 \pm 1.49$	$-10.65 \pm 2.89$

 $<sup>^{</sup>a}\Delta G_{\text{MM-GB/SA}} = E_{\text{ele}} + E_{\text{vdw}} + \Delta G_{\text{GB}} + \Delta G_{\text{SASA}}$ 

Table 2. Decomposition energies of some important residues in HSP47:collagen complex (kcal·mol<sup>-1</sup>).

Residue	$E_{ m vdw}$	$E_{ m ele}$	$\Delta G_{GB}$	$\Delta G_{SASA}$	$E_{\text{total}}$
Met218	-3.15	-0.34	1.04	-0.52	-2.97
His238	-2.36	-1.10	1.70	-0.21	-1.97
His274	-2.17	-4.77	5.54	-0.40	-1.80
Leu381	-2.29	0.29	0.67	-0.47	-1.80
Tyr383	-3.35	-2.71	3.77	-0.38	-2.67
Asp385	0.19	-53.82	51.43	-0.28	-2.48
A_pro7	-0.79	0.24	-0.39	-0.12	-1.06
A_pro10	-2.45	-0.85	1.07	-0.40	-2.63
A_pro13	-1.45	0.40	-0.34	-0.28	-1.67
A_pro14	-1.61	-0.21	0.39	-0.36	-1.79
B_pro4	-2.16	-1.59	2.11	-0.39	-2.03
B_pro7	-3.86	-0.34	0.72	-0.55	-4.03
B_thr8	-3.00	-6.55	4.08	-0.63	-6.1
B_pro10	-1.87	-0.69	0.75	-0.24	-2.05
B_arg11	-1.78	-19.08	15.22	-0.65	-6.29
C_pro2	-2.13	-0.89	1.16	-0.48	-2.34

It was considered that the residue had interaction with other components when the  $E_{\text{total}}$  lower than  $-1 \, \text{kcal mol}^{-1}$ . Uppercase amino acid letter indicated residues from receptor (HSP47), and lowercase amino acid letter indicated residues from ligands (collagen/SCi), the same below.

corresponding HSP47 residues were also neutral amino acids. Only one polar residue Asp385 of HSP47 contributed -2.48 kcal·mol<sup>-1</sup> to the collagen model binding (Figure 3(B), Table 2), Conversely, when SCi bound to HSP47, the charged amino acids (Arg222, Arg228, Asp247, Glu249, Lys252, Arg377) of HSP47 around the binding site of collagen model activated by SCi (Figure 3(D), Table 3).

#### Conformational variation of SCi and SCd

We extracted the average structures to superimpose free SCi and SCd, SCi and SCd from complexes, respectively, and observed the movement of Ca<sup>2+</sup> binding loop intuitively. When  $Ca^{2+}$  located in SCd, the conformations of the four loops (residues no. 20-33, 63-74 of either chain A or chain B) (Figures 3(F,G) and 5) were changed comparing with SCi. In SCd, the binding site was prone to keep loop conformation. Once without Ca<sup>2+</sup> in SCi, these residues were easier to form  $\alpha$ -helix (red),  $\beta$ -sheet (cyan) and  $\beta$ -turn (green) (Figure 5).

To further investigate the structural alternation of SCi/ SCd, we calculated root mean square fluctuation (RMSF) values of Cα atoms for free or binding SCi/SCd to evaluate the flexibility of backbones during MD simulation (Figure 6). In the first peak (Figure 6, from left to right, the same below) of residues from 19 to 30 of chain A, where a Ca<sup>2+</sup> located, the chains of SCd and free SCi were more flexible than that of SCi in HSP47:SCi complex. Lys22 of SCi chain A had evident affinity to HSP47 (Table 3). Both the second and the

Table 3. Decomposition energies of some important residues in HSP47:SCi complex (kcal·mol<sup>-1</sup>).

Residue	$E_{ m vdw}$	$E_{\mathrm{ele}}$	$\Delta G_{GB}$	$\Delta G_{SASA}$	$E_{ m total}$
Arg222	-0.67	-55.45	53.60	-0.39	-2.91
Met225	-1.72	-0.32	0.60	-0.45	-1.89
Arg228	-0.24	-112.81	100.59	-1.06	-13.52
Asp247	-0.04	9.94	-12.14	-0.19	-2.43
Glu249	-1.71	8.87	-9.81	-0.57	-3.22
Lys252	-0.72	-52.58	51.90	-0.27	-1.67
His273	-3.02	0.11	2.26	-0.35	-1.00
His274	-3.49	-10.10	9.75	-0.63	-4.47
Val275	-1.13	-1.37	1.10	-0.17	-2.67
Arg377	-3.27	-96.55	96.60	-0.53	-3.75
Leu381	-3.10	-1.65	2.44	-0.73	-3.04
A_lys22	-0.28	-26.99	21.63	-0.48	-6.12
A_arg40	-3.96	-18.03	16.94	-0.60	-5.65
A_glu91	0.82	-79.13	76.60	-0.23	-1.94
B_tyr3	-2.34	-2.18	3.26	-0.23	-1.49
B_pro4	-1.33	-2.15	2.27	-0.25	-1.46
B_glu6	0.17	-47.68	46.57	-0.19	-1.13
B_phe89	-2.78	-0.23	1.93	-0.52	-1.60
B_phe90	-2.88	-4.25	5.01	-0.46	-2.58
B_glu91	-1.27	-38.01	38.39	-0.22	-1.11

fifth peaks (residues 44-53 of chain A, 45-59 of chain B, respectively) were the linking loops between two EF-hand motifs. The third peak referred to the terminals between two single chains of SCi/SCd, which RMSF values were extremely high in all structures. The fourth peak was the backbone of residues from 19 to 29 of chain B, which directed to another Ca<sup>2+</sup> binding loop. In the presence of HSP47, most of the fluctuation of backbone was much lower than that in free SCi.

The PCA calculation could provide a convenient framework to identify concerted, nonrandom fluctuations in the presence of structures. The results of the correlation calculations characterized the linear correlation between any pair of Cα atoms in SCi/SCd as they moved near their average positions during MD simulations (Figure 7). To identify the movement of SCi/SCd in a concerted fashion depending on Ca<sup>2+</sup> binding, the cross-correlation coefficients of pairs of SCi/SCd residues were analyzed based on the MD trajectories of SCi/ SCd structures.

#### **Discussion**

In the present study, we found SCi could bind with HSP47 in the AP cells. This phenomenon has not been reported in the literature, suggesting that S100A4 may play novel roles in the AP cells. We discussed the aspects following: 1. the general structural characteristics and functions of HSP47 and SCi/SCd; 2. the MD and energetic distinctions among

 $<sup>{}^{\</sup>rm b}\Delta G_{\rm TOT} = \Delta G_{\rm MM-GB/SA} - T\Delta S.$ 

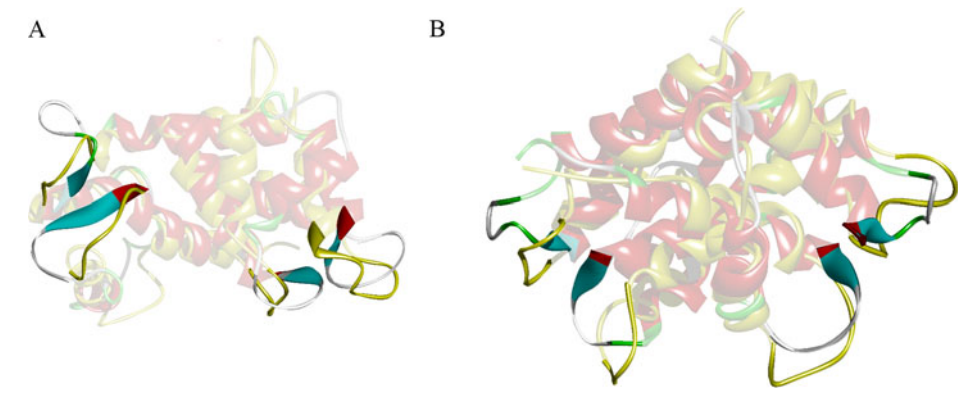


Figure 5. Colored chains were SCi and the yellow ones were SCd. The non-transparent parts were the loops interacting with Ca<sup>2+</sup>. (A) The overlap between free SCi and SCd, the RMSD value is 5.21 Å. (B) The overlap between SCi and SCd from complexes, the RMSD value is 4.68 Å.

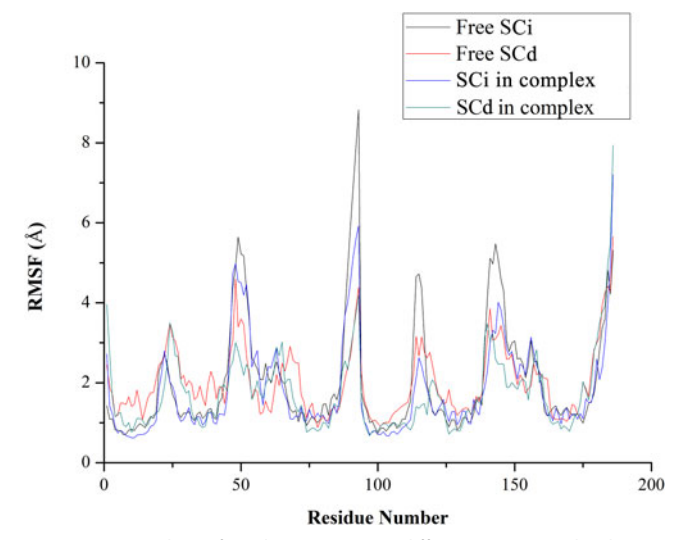


Figure 6. RMSF values of residue  $C\alpha$  atoms in different S100A4 molecules.

HSP47:collagens, HSP47:SCi and HSP47:SCd complexes; 3. the conformational variation of SCi/SCd structures; 4. the research meaning of our study on antler biology.

According to the BLAST search, 3ZHA.A, 3KO0.A and 2KLW were chosen as the final template structure for several reasons: 3ZHA.A and 3KO0.A both had high similarity with the target sequences. Most of the QMEANDisCo score were higher than 0.6, which means the models were more reasonable for further simulation. Besides, S100A4 dimer had different combination mode in crystal structures. We selected the activated form containing four Ca<sup>2+</sup>s to build the homology model. Ensuring the coordinates of Ca<sup>2+</sup>s were accurate in SCd model.

Various binding modes between HSP47 and collagens/ SCi/SCd were observed based on HSP47:collagens, HSP47:SCi and HSP47:SCd models. In collagens, a GLY-X-Y triplet repetitive sequence is necessary for HSP47 to recognize (Ono, Miyazaki, Ishida, Uehata, & Nagata, 2012). We also defined the binding site of HSP47 (Widmer et al., 2012) to dock collagens. However, when HSP47 docked with SCi/SCd, there were no foregone binding sites presented in HSP47. So we had to perform a random docking method between HSP47 and SCi/SCd, and adopt the structures with lowest zrank

score for the subsequent MD simulation. Coincidentally, the docking results showed that SCi and SCd with lowest score almost occupied the binding site between HSP47 and collagen model. Moreover, it seems that the Ca<sup>2+</sup>s did not have much effect to change the binding surface of SCd. A SCi/SCd molecule exists as homodimer intracellularly, which is composed of two single chains (A and B). A subunit of SCd contains two EFhands, each of which can interact with two Ca<sup>2+</sup>s (Pathuri, Vogeley, & Luecke, 2008). However, HSP47 was not a symmetric structure itself, which approached to chain A rather than chain B (Figure 3(C,E)). These results mean that HSP47 could exert different influence on either chain of SCi/SCd.

There are various studies on the signaling pathways regulating the ECM accumulation, stiffness and remodeling during cancer process extracellularly (Fang, Yuan, Peng, & Li, 2014; Kojima et al., 2010; Provenzano, Inman, Eliceiri, & Keely, 2009). In our present research, we focused on the collagen assembly and secretion with S100A4 participation intracellularly (Figure 8). HSP47 had higher affinity to SCi than to collagens. Mature type I, III collagens are the structural component of ECM, and collagen IV is the basal reticular matrix of basement membrane (BM) (Couchman, Beavan, & Mccarthy, 1994). In early stage of cancers, TGF-β pathway were stimulated (Bellomo, Caja, & Moustakas, 2016), causing type I, III collagens be synthesized and secreted into intercellular substance. Together with BM, cross-linked collagen network is constituted as barrier against epithelial-tomesenchymal transition (EMT) (Coleman & Eccles, 1997; Westermarck & Kähäri, 1999; Butcher, Alliston, & Weaver, 2009). However, the over-accumulation of collagen results in ECM stiffness and is ready for metastasis of tumor cells (Wozniak, Desai, Solski, Der, & Keely, 2003). With cancer stage becoming advanced, S100A4 and matrix metalloproteinases (MMPs) were activized in turn. In general, HSP47 is necessary for collagen to assemble and fold correctly (Chu et al., 2015). When molecular chaperone effect of HSP47 is interfered by S100A4, the collagen is misfolded intracellularly and remodeled radially by MMPs extracellularly (Bonnans, Chou, & Werb, 2014). The stiff ECM is thus converted to be advantageous for cell migration due to the ECM remodeled (Zhang, Liu, Hao, Dong, & Chen, 2016). Besides, MMP-2/9 can degrade collagen IV specifically. The agents above cause the EMT process happening (Kalluri & Zeisberg, 2006).

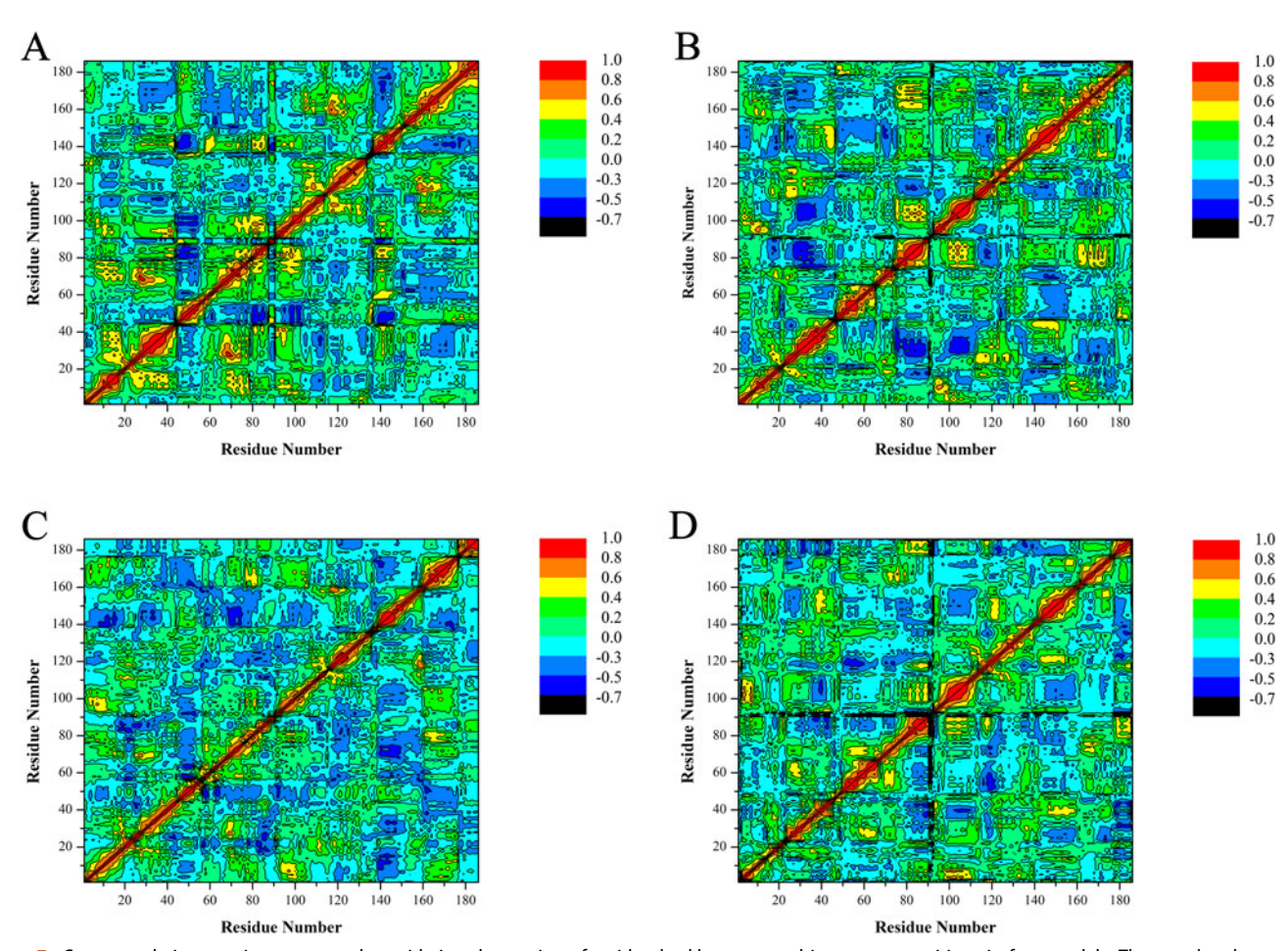


Figure 7. Cross-correlation matrices computed considering the motion of residue backbone around its average positions in four models. The correlated extent of motions between atoms is displayed in color-coded modes. The red to yellow color represents a strong positive correlation between atoms corresponding to a concerted motion along the same direction. The blue and dark blue color shows a negative correlation between atoms reflecting motion in the opposite direction. (A) Free SCi, (B) free SCd, (C) subunit of SCi from HSP47:SCi complex, (D) subunit of SCd from HSP47:SCd complex.

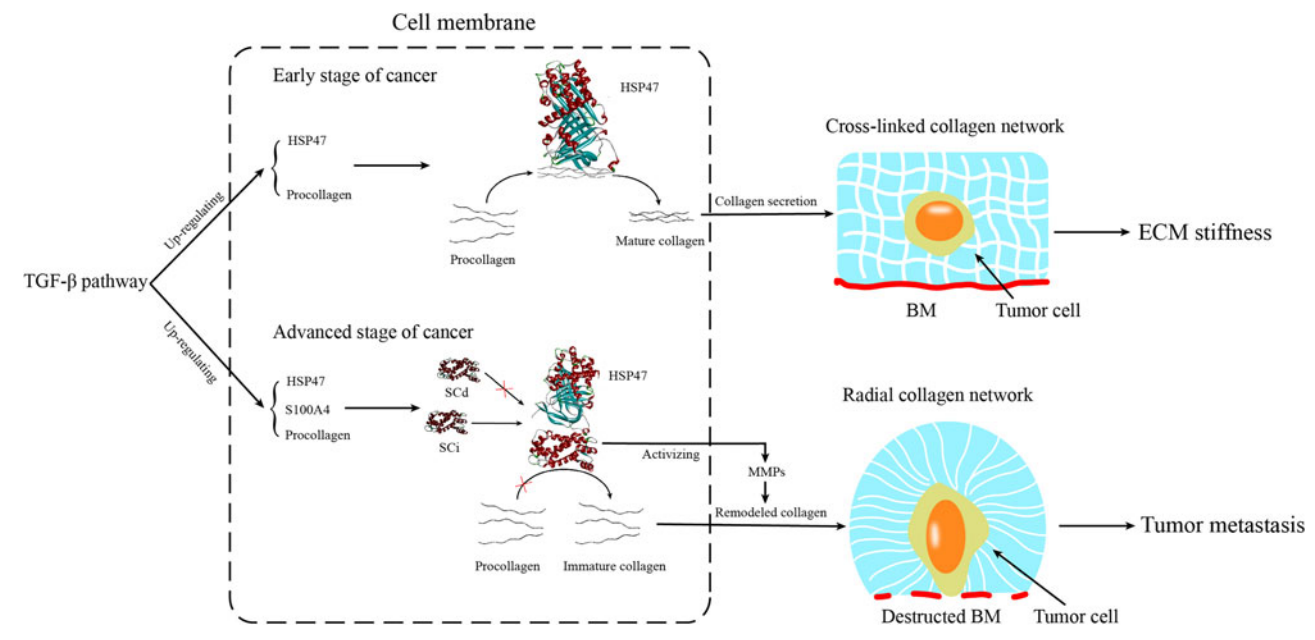


Figure 8. The process of collagen synthesis during different stages of cancer.

The binding free energies showed that the incorporating intensity distinct among the HSP47:collagens, were HSP47:SCi and HSP47:SCd complexes. Natsume et al. reported that HSP47 can bind newly synthesized procollagen and facilitate the mature collagen transported from ER to Golgi vesicle (Natsume, Koide, Yokota, Hirayoshi, & Nagata,

1994). The binding between HSP47 and collagen is rapid association/dissociation process. Our results were coincidental with the experimental data (Table 1). The low energies of HSP47:collagens indicating the faint affinity between the two components was not differential. Therefore, the binding between HSP47 and collagen was a transient course. Comparing with the stronger binding between HSP47 and SCi, the interaction of HSP47 and collagens were much weaker, which means that SCi could compete with the binding site of HSP47 actively. Surprisingly, SCd had little interaction with HSP47, indicating that incorporation of Ca<sup>2+</sup> may not be beneficial for the binding. So we suspect that binding of S100A4 with HSP47 was a Ca<sup>2+</sup>-independent process.

Combining the results of Ca<sup>2+</sup> binding loop variation (Figure 5), RMSF plots (Figure 6), and cross-correlation matrices of PCA (Figure 7), we found some interesting agents that could influence the conformational change of the SCi/SCd structures during the MD simulations: (1) in the structure of free SCi, the  $\alpha$ -helices in chain A were the components of EF-hand motif. They seem to have the same pattern of movement. The Ca<sup>2+</sup> binding loops also moved to the same direction. However, the motions of some  $\alpha$ -helices in chain B were opposite to the ones in chain A. Besides, the linking loops between two EF-hand motifs were highly flexible zones, which moved different direction towards the N-terminal of the chain B and other linking loops (Figure 7(A)); (2) with the incorporation of Ca<sup>2+</sup>s, the motion of free SCd was distinct from the free SCi. The  $\alpha$ -helices composing of EFhands were converted to orient different direction each other. In general, regular secondary structure benefits for stability of conformation because of the inter residue hydrogen bonds. However, in free SCd, loops of EF-hand were more appropriate for Ca<sup>2+</sup> binding, and profited to increase structural stability. From the appearances that free SCd presented, we found that Ca<sup>2+</sup> could change the conformation of EFhand motif following affect the whole structure of SCd. This may be the basic reason for multiple biological activity of SCi/SCd. (Figure 7(B)); (3) when SCi binding with HSP47, the flexibility of the linking loop between consecutive EF-hand motifs was restrained by HSP47, further restricted the movement of whole EF-hand motif in chain A. Chain B was acquired more degree of freedom relatively, instead. More of the chain B residues participated the binding with HSP47 than that of the chain A (Table 3, Figure 7(C)); (4) in HSP47:SCd complex, most of  $C\alpha$  atoms movement of SCd was less fluctuating than that of free SCd. Besides, some intramolecular α-helices had slight relative motion, which presented more rigid in whole structural scale than the former ones under the combined action of Ca<sup>2+</sup> and HSP47. We considered that the lower flexibility of SCd was the reason for the little interaction when SCd docking with HSP47 (Table 1, Figure 7(D)).

Highly expressed S100A4 could stimulate angiogenesis and cell proliferation in antler growth, but not migration in the AP , PP or RM cells (Wang et al., 2017). Histologically, antler development from the AP can be divided into four stages (Li & Suttie, 1994): intramembranous ossification (IMO), ossification pattern change (OPC), pedicle

endochondral ossification (pECO), and antler endochondral ossification (aECO). The AP cells differentiate into various progenies in each stage. However, in the AP cells, with the interference of SCi, HSP47 may not execute the function of assembling collagens, causing abundant immature and abnormal appearance of collagen secreted out of cells. MMPs which are also activated by S100A4 (Mathisen et al., 2003) participate the remodeling of collagens (Sillat et al., 2012; Somaiah et al 2015). With the two factors combined, the microenvironment is advantageous and prepared for stationary phase the AP cells to proliferate and differentiate in the IMO stage (Li & Suttie, 2001). On the basis of our study about S100A4 and HSP47, we will explore the inherent connections between ECM and S100A4 extracellularly during proliferation and differentiation of the AP, PP and RM cells.

#### **Conclusion**

We found S100A4 could bind with HSP47 in AP cells using co-immunoprecipitation assay. MD simulation indicated that this was a Ca<sup>2+</sup>-independent process for S100A4. Following studies showed that Ca<sup>2+</sup> and HSP47 could influence the conformational change of SCi/SCd greatly. Based on our research, we speculated that the interaction between SCi and HSP47 induced the remodeling of ECM and BM, further improve the microenvironment for AP cells differentiation. This work is expected to provide significant dynamical information involving conformational changes of SCi/SCd for the further investigation on the development of AP , PP and RMcells or other similar S100A4 over-expression cells.

#### **Disclosure statement**

The authors declared no potential conflicts of interest with respect to the research, authorship, and/or publication of this article.

#### References

Bellomo, C., Caja, L., & Moustakas, A. (2016). Transforming growth factor β as regulator of cancer stemness and metastasis. *British Journal of Cancer*, *115*(7), 761–769. doi:10.1038/bjc.2016.255

Benkert, P., Biasini, M., & Schwede, T. (2011). Toward the estimation of the absolute quality of individual protein structure models. *Bioinformatics*, 27(3), 343–350. doi:10.1093/bioinformatics/btq662

Biasini, M., Bienert, S., Waterhouse, A., Arnold, K., Studer, G., Schmidt, T., ... Schwede, T. (2014). Swiss-model: Modelling protein tertiary and quaternary structure using evolutionary information. *Nucleic Acids Research*, 42(W1), W252–W258. doi:10.1093/nar/gku340

Bonnans, C., Chou, J., & Werb, Z. (2014). Remodelling the extracellular matrix in development and disease. *Nature Reviews Molecular Cell Biology*, *15*(12), 786–801. doi:10.1038/nrm3904

Boye, K., & Maelandsmo, G. M. (2010). S100a4 and metastasis: A small actor playing many roles. *The American Journal of Pathology*, *176*(2), 528–535. doi:10.2353/ajpath.2010.090526

Butcher, D. T., Alliston, T., & Weaver, V. M. (2009). A tense situation: Forcing tumour progression. *Nature Reviews Cancer*, 9(2), 108–122. doi:10.1038/nrc2544

Case, D. A., Berryman, J. T., & Betz, R. M. (2015). *AMBER 2015*. San Francisco, CA: University of California.

Chen, J., Wang, X., Zhu, T., Zhang, Q., & Zhang, J. Z. (2015). A comparative insight into amprenavir resistance of mutations v32i, g48v, i50v, i54v, and i84v in hiv-1 protease based on thermodynamic integration

- and mm-pbsa methods. Journal of Chemical Information and Modeling, 55(9), 1903-1913. doi:10.1021/acs.jcim.5b00173
- Chu, H., Wu, T., Wu, W., Tu, W., Jiang, S., Chen, S., & Wang, J. (2015). Involvement of collagen-binding heat shock protein 47 in scleroderma-associated fibrosis. Protein & Cell, 6(8), 589-598. doi:10.1007/ s13238-015-0171-3
- Coleman, R. E., & Eccles, S. A. (1997). General mechanisms of metastasis. Cancer, 80(8 Suppl), 1529-1537.
- Coleman, T. G., Mesick, H. C., & Darby, R. L. (1977). Numerical integration. Annals of Biomedical Engineering, 5(4), 322-328. doi:10.1007/ BF02367312
- Couchman, J. R., Beavan, L. A., & Mccarthy, K. J. (1994). Glomerular matrix: Synthesis, turnover and role in mesangial expansion. Kidney International, 45(2), 328-335. doi:10.1038/ki.1994.42
- Deb-Choudhury, S., Wang, W., Clerens, S., McMahon, C., Dyer, J. M., & Li, C. (2015). Direct localisation of molecules in tissue sections of growing antler tips using MALDI imaging. Molecular and Cellular Biochemistry, 409(1-2), 225-241. doi:10.1007/s11010-015-2527-7
- Duan, L. L., Feng, G. Q., & Zhang, Q. G. (2016). Large-scale molecular dynamics simulation: Effect of polarization on thrombin-ligand binding energy. Scientific Reports, 6, 31488.
- Essmann, U., Perera, L., Berkowitz, M. L., Darden, T., Lee, H., & Pedersen, L. G. (1995). A smooth particle mesh Ewald method. Journal of Chemical Physics, 103(19), 8577-8593. doi:10.1063/1.470117
- Fang, M., Yuan, J., Peng, C., & Li, Y. (2014). Collagen as a double-edged sword in tumor progression. Tumour Biology: The Journal of the International Society for Oncodevelopmental Biology and Medicine, 35(4), 2871-2882. doi:10.1007/s13277-013-1511-7
- Garrett, S. C., Varney, K. M., Weber, D. J., & Bresnick, A. R. (2006). S100a4, a mediator of metastasis. The Journal of Biological Chemistry, 281(2), 677-680. doi:10.1074/jbc.R500017200
- Goss, R. J. (1990). Of Antlers and Embryos. Horns, Pronghorns, and Antlers (pp. 298-312). New York, NY: Springer.
- Helfman, D. M., Kim, E. J., Lukanidin, E., & Grigorian, M. (2005). The metastasis associated protein s100a4: Role in tumour progression and metastasis. British Journal of Cancer, 92(11), 1955-1958. doi:10.1038/sj. bjc.6602613
- Hirayoshi, K., Kudo, H., Takechi, H., Nakai, A., Iwamatsu, A., Yamada, K. M., & Nagata, K. (1991). Hsp47: A tissue-specific, transformation-sensitive, collagen-binding heat shock protein of chicken embryo fibroblasts. Molecular and Cellular Biology, 11(8), 4036-4044. doi:10.1128/ MCB.11.8.4036
- Hornak, V., Abel, R., Okur, A., Strockbine, B., Roitberg, A., & Simmerling, C. (2006). Comparison of multiple amber force fields and development of improved protein backbone parameters. Proteins: Structure, Function, and Bioinformatics, 65(3), 712-725. doi:10.1002/prot.21123
- Hou, T., Zhang, W., Case, D. A., & Wang, W. (2008). Characterization of domain-peptide interaction interface: A case study on the amphiphysin-1 sh3 domain. Journal of Molecular Biology, 376(4), 1201–1214. doi: 10.1016/j.jmb.2007.12.054
- Humphrey, W., Dalke, A., & Schulten, K. (1996). Vmd: Visual molecular dynamics. Journal of Molecular Graphics, 14(1), 33-38. doi:10.1016/ 0263-7855(96)00018-5
- Hwang, H., Vreven, T., Janin, J., & Weng, Z. (2010). Protein-protein docking benchmark version 4.0. Proteins: Structure, Function, and Bioinformatics, 78(15), 3111-3114. doi:10.1002/prot.22830
- Ichiye, T., & Karplus, M. (1991). Collective motions in proteins: A covariance analysis of atomic fluctuations in molecular dynamics and normal mode simulations. Proteins: Structure, Function, and Genetics, 11(3), 205-217. doi:10.1002/prot.340110305
- Jorgensen, W. L., Chandrasekhar, J., Madura, J. D., Impey, R. W., & Klein, M. L. (1983). Comparison of simple potential functions for simulating liquid water. Journal of Chemical Physics, 79(2), 926-935. doi:10.1063/ 1.445869
- Kalluri, R., & Zeisberg, M. (2006). Fibroblasts in cancer. Nature Reviews Cancer, 6(5), 392-401. doi:10.1038/nrc1877
- Kim, E. J., & Helfman, D. M. (2003). Characterization of the metastasisassociated protein, s100a4. roles of calcium binding and dimerization in cellular localization and interaction with myosin. Journal of

- Biological Chemistry, 278(32), 30063-30073. doi:10.1074/jbc. M304909200
- Kojima, Y., Acar, A., Eaton, E. N., Mellody, K. T., Scheel, C., Ben-Porath, I., ... Orimo, A. (2010). Autocrine tgf-beta and stromal cell-derived factor-1 (sdf-1) signaling drives the evolution of tumor-promoting mammary stromal myofibroblasts. Proceedings of the National Academy of Sciences of the United States of America, 107(46), 20009-20014. doi:10. 1073/pnas 1013805107
- Laskowski, R. A., Macarthur, M. W., Moss, D. S., & Thornton, J. M. (1993). PROCHECK: A program to check the stereochemical quality of protein structures. Journal of Applied Crystallography, 26(2), 283-291. doi:10. 1107/S0021889892009944
- Li, C., Clark, D. E., Lord, E. A., Stanton, J. A., & Suttie, J. M. (2002). Sampling technique to discriminate the different tissue layers of growing antler tips for gene discovery. The Anatomical Record, 268(2), 125-130. doi:10.1002/ar.10120
- Li, C., Mackintosh, C. G., Martin, S. K., & Clark, D. E. (2007a). Identification of key tissue type for antler regeneration through pedicle periosteum deletion. Cell and Tissue Research, 328(1), 65-75. doi:10.1007/s00441-006-0333-v
- Li, C., Stanton, J. A. L., Robertson, T. M., Suttie, J. M., Sheard, P. W., Harris, A. J., & Clark, D. E. (2007b). Nerve growth factor mrna expression in the regenerating antler tip of red deer (Cervus elaphus). PLoS One, 2(1), e148. doi:10.1371/journal.pone.0000148
- Li, C., & Suttie, J. M. (1994). Light microscopic studies of pedicle and early first antler development in red deer (Cervus elaphus). The Anatomical Record, 239(2), 198-215. doi:10.1002/ar.1092390211
- Li, C., & Suttie, J. M. (2001). Deer antlerogenic periosteum: A piece of postnatally retained embryonic tissue? Anatomy and Embryology, 204(5), 375-388, doi:10.1007/s004290100204
- Li, C., Yang, F., & Sheppard, A. (2009). Adult stem cells and mammalian epimorphic regeneration-insights from studying annual renewal of deer antlers. Current Stem Cell Research & Therapy, 4(3), 237-251. doi: 10.2174/157488809789057446
- Li, C., Yang, F., & Suttie, J. (2011). Stem cells, stem cell niche and antler development. Animal Production Science, 51(4), 267-276. doi:10.1071/ AN10157
- Li, C., Zhao, H., Liu, Z., & Mcmahon, C. (2014). Deer antler-a novel model for studying organ regeneration in mammals. The International Journal of Biochemistry & Cell Biology, 56, 111-122. doi:10.1016/j.biocel.2014.07.007
- Li, P., Roberts, B. P., Chakravorty, D. K., & Merz, K. M. Jr. (2013). Rational design of particle mesh ewald compatible lennard-jones parameters for +2 metal cations in explicit solvent. Journal of Chemical Theory and Computation, 9(6), 2733-2748. doi:10.1021/ct400146w
- Mathisen, B., Lindstad, R. I., Hansen, J., El-Gewely, S. A., Maelandsmo, G. M., Hovig, E., & Winberg, J. O. (2003). S100a4 regulates membrane induced activation of matrix metalloproteinase-2 in osteosarcoma cells. Clinical & Experimental Metastasis, 20(8), 701-711. doi:10.1023/ B:CLIN.0000006819.21361.03
- Merklinger, S. L., Wagner, R. A., Spiekerkoetter, E., Hinek, A., Knutsen, R. H., Kabir, M. G., ... Rabinovitch, M. (2005). Increased fibulin-5 and elastin in s100a4/mts1 mice with pulmonary hypertension. Circulation Research, 97(6), 596-604. doi:10.1161/01.RES.0000182425.49768.8a
- Miller, B. R., III, McGee, T. D., Jr, Swails, J. M., Homeyer, N., Gohlke, H., & Roitberg, A. E. (2012). Mmpbsa.py: An efficient program for end-state free energy calculations. Journal of Chemical Theory and Computation, 8(9), 3314-3321. doi:10.1021/ct300418h
- Minowada, G., & Welch, W. J. (1995). Clinical implications of the stress response. Journal of Clinical Investigation, 95(1), 3-12.
- Nagata, K. (1998). Expression and function of heat shock protein 47: A collagen-specific molecular chaperone in the endoplasmic reticulum. Matrix Biology, 16(7), 379-386. doi:10.1016/S0945-053X(98)90011-7
- Natsume, T., Koide, T., Yokota, S., Hirayoshi, K., & Nagata, K. (1994). Interactions between collagen-binding stress protein hsp47 and collagen. analysis of kinetic parameters by surface plasmon resonance biosensor. Journal of Biological Chemistry, 269(49), 31224-31228.
- Ono, T., Miyazaki, T., Ishida, Y., Uehata, M., & Nagata, K. (2012). Direct in vitro and in vivo evidence for interaction between hsp47 protein and



- collagen triple helix. Journal of Biological Chemistry, 287(9), 6810-6818. doi:10.1074/jbc.M111.280248
- Pathuri, P., Vogeley, L., & Luecke, H. (2008). Crystal structure of metastasis-associated protein s100a4 in the active calcium-bound form. Journal of Molecular Biology, 383(1), 62-77. doi:10.1016/j.jmb.2008.04.
- Pedersen, M. V., Køhler, L. B., Grigorian, M., Novitskaya, V., Bock, E., Lukanidin, E., & Berezin, V. (2004). The mts1/s100a4 protein is a neuroprotectant. Journal of Neuroscience Research, 77(6), 777-786. doi:10. 1002/inr.20221
- Pierce, B. G., Hourai, Y., & Weng, Z. (2011). Accelerating protein docking in zdock using an advanced 3d convolution library. PLoS One, 6(9), e24657. doi:10.1371/journal.pone.0024657
- Provenzano, P. P., Inman, D. R., Eliceiri, K. W., & Keely, P. J. (2009). Matrix density-induced mechanoregulation of breast cell phenotype, signaling, and gene expression through a fak-erk linkage. Oncogene, 28(49), 4326-4343. doi:10.1038/onc.2009.299
- Roe, D. R., & Cheatham, T. E., III. (2013). Ptraj and cpptraj: Software for processing and analysis of molecular dynamics trajectory data. Journal of Chemical Theory and Computation, 9(7), 3084-3095. doi:10. 1021/ct400341p
- Santamaria-Kisiel, L., Rintala-Dempsey, A. C., & Shaw, G. S. (2006). Calcium-dependent and -independent interactions of the s100 protein family. Biochemical Journal, 396(2), 201-214. doi:10.1042/BJ20060195
- Schmidt-Hansen, B., Klingelhöfer, J., Grum-Schwensen, B., Christensen, A., Andresen, S., Kruse, C., ... Grigorian, M. (2004). Functional significance of metastasis-inducing s100a4(mts1) in tumor-stroma interplay. Journal of Biological Chemistry, 279(23), 24498-24504. doi:10.1074/jbc. M400441200
- Sillat, T., Saat, R., Pöllänen, R., Hukkanen, M., Takagi, M., & Konttinen, Y. T. (2012). Basement membrane collagen type iv expression by human mesenchymal stem cells during adipogenic differentiation. Journal of Cellular and Molecular Medicine, 16(7), 1485-1495. doi:10. 1111/j.1582-4934.2011.01442.x
- Somaiah, C., Kumar, A., Mawrie, D., Sharma, A., Patil, S. D., Bhattacharyya, J., ... Jaganathan, B. G. (2015). Collagen promotes higher adhesion, survival and proliferation of mesenchymal stem cells. PLoS One, 10(12), e0145068. doi:10.1371/journal.pone.0145068

- Swanson, J. M. J., Henchman, R. H., & Mccammon, J. A. (2004). Revisiting free energy calculations: A theoretical connection to mm/pbsa and direct calculation of the association free energy. Biophysical Journal, 86(1), 67-74, doi:10.1016/S0006-3495(04)74084-9
- Tarabykina, S., Griffiths, T. R., Tulchinsky, E., Mellon, J. K., Bronstein, I. B., & Kriajevska, M. (2007). Metastasis-associated protein s100a4: Spotlight on its role in cell migration. Current Cancer Drug Targets, 7(3), 217-228. doi:10.2174/156800907780618329
- Wang, D. T., Chu, W. H., Sun, H. M., Ba, H. X., & Li, C. Y. (2017). Expression and functional analysis of tumor-related factor s100a4 in antler stem cells. Journal of Histochemistry & Cytochemistry Official Journal of the Histochemistry Society, 65(10), 22155417727263.
- Westermarck, J., & Kähäri, V. M. (1999). Regulation of matrix metalloproteinase expression in tumor invasion. FASEB Journal Official Publication of the Federation of American Societies for Experimental Biology, 13(8), 781-792. doi:10.1096/fasebj.13.8.781
- Widmer, C., Gebauer, J. M., Brunstein, E., Rosenbaum, S., Zaucke, F., Drogemuller, C., ... Baumann, U. (2012). Molecular basis for the action of the collagen-specific chaperone hsp47/serpinh1 and its structure-specific client recognition. Proceedings of the National Academy of Sciences of the United States of America, 109(33), 13243-13247. doi:10.1073/pnas.1208072109
- Wong, M. M., Yin, X., Potter, C., Yu, B., Cai, H., Di Bernardini, E., & Xu, Q. (2014). Over-expression of HSP47 augments mouse embryonic stem cell smooth muscle differentiation and chemotaxis. PLoS One, 9(1), e86118. doi:10.1371/journal.pone.0086118
- Wozniak, M. A., Desai, R., Solski, P. A., Der, C. J., & Keely, P. J. (2003). Rock-generated contractility regulates breast epithelial cell differentiation in response to the physical properties of a three-dimensional collagen matrix. The Journal of Cell Biology, 163(3), 583-595. doi:10. 1083/jcb.200305010
- Xu, R. (2015). MiR-29/HSP47 in ECM network. Oncoscience, 2(10), 843-844. doi:10.18632/oncoscience.227
- Zhang, K., Liu, X., Hao, F., Dong, A., & Chen, D. (2016). Targeting tgf-\u00ed1 inhibits invasion of anaplastic thyroid carcinoma cell through smad2dependent s100a4-mmp-2/9 signalling. American Journal of Translational Research, 8(5), 2196-2209.